Title

Tuning charge density wave order and superconductivity in the kagome metals KV3Sb5âxSnx
and
RbV3Sb5âxSnx

Journal

Physical Review Materials, 6(7)

ISSN

2475-9953

Authors

Oey, Yuzki M
Kaboudvand, Farnaz
Ortiz, Brenden R
et al.

Publication Date

2022-07-13

DOI

10.1103/PhysRevMaterials.6.074802

Peer reviewed

Tuning charge-density wave order and superconductivity in the kagome metals $KV_3Sb_{5-x}Sn_x$ and $RbV_3Sb_{5-x}Sn_x$

Yuzki M. Oey,[1] Farnaz Kaboudvand,[1] Brenden R. Ortiz,[1] Ram Seshadri,[1] and Stephen D. Wilson[1]

[1]*Materials Department, Materials Research Laboratory, and California NanoSystems Institute University of California Santa Barbara, California 93106 United States**

(Dated: April 22, 2022)

The family of AV_3Sb_5 (A = K, Rb, Cs) kagome metals exhibit chiral charge density wave (CDW) order followed by a superconducting state. Recent studies have shown the importance that band structure saddle points proximal to the Fermi energy play in governing these two transitions. Here we show the effects of hole-doping achieved *via* chemical substitution of Sn for Sb on the CDW and superconducting in both KV_3Sb_5 and RbV_3Sb_5, and generate a phase diagram. Lifting the Γ pocket and van Hove singularities (vHs) across E_F causes the superconducting T_C in both systems to increase to about 4.5 K, while rapidly suppressing the CDW transitions.

INTRODUCTION

Structures with kagome nets inherently host electronic instabilities that lead to a variety of interesting phases, including topological insulators,[1] unconventional superconductivity,[2] and Weyl semimetal states [3]. The AV_3Sb_5 (A: K, Rb, Cs) class of kagome metals [4] show many of these unconventional states and are candidates to study the interplay between charge density wave (CDW) order and superconductivity (SC) [5–7]. Recently, the effects of making small changes to the electronic band structures on SC and CDW ordering have been studied computationally [8, 9] and experimentally by applying external hydrostatic pressure [10–13] and hole doping on various sites [14].

The electron pocket comprising Sb p orbitals at Γ, and saddle points arising from V d-orbitals at M-points are regarded as being important to the SC and CDW states and consequently, understanding their behavior when subject to external perturbations such as pressure and chemical doping is important to understand. Recently, we reported the effect of hole doping in CsV_3Sb_5 with Sn substituting Sb, and observed a double superconducting dome that we attributed to the lifting of the Γ pocket above E_F. The van Hove singularities (vHs) at the M point are lifted with the substitution resulting in rapid suppression of the CDW transition [14]. While external applied pressure moves the M saddle points away from E_F, hole-doping the systems moves the Γ pocket and vHs points up through E_F [8]. Despite these differences, it is interesting to note that the observed changes in SC and CDW are similar in both pressure and hole-doping studies. In CsV_3Sb_5, two peaks in SC T_C are observed with a suppressed and eventually disappearing CDW transition with both low applied pressure ($P < 5$ GPa) [11] and hole-doping on the Sb site [14]. Conversely, pressure studies have reported a single superconducting dome in KV_3Sb_5 and RbV_3Sb_5 [10, 12].

Here the effect of hole doping AV_3Sb_5 with in solid solutions with A = K, Rb is presented. In both systems, only one superconducting dome is observed in contrast with $CsV_3Sb_{5-x}Sn_x$, although a similar CDW suppression is observed. The solubility limit of Sn in KV_3Sb_5 is the lowest in the family, with phase separation observed by $x = 0.30$. In contrast RbV_3Sb_5 supports up to $x = 0.70$ of Sn replacing Sb. While the differences in solubility can be explained by A cation size effects, the different SC and CDW behavior must be attributed to subtle differences in band structure. Recent optical measurements coupled with density functional theory (DFT) calculations have shown that the saddle points around M are slightly rearranged between CsV_3Sb_5 and KV_3Sb_5 [8, 9], which may lead to the differences observed in superconductivity enhancement.

EXPERIMENTAL DETAILS

Powder samples of $KV_3Sb_{5-x}Sn_x$ and $RbV_3Sb_{5-x}Sn_x$ for $0 \leq x \leq 1$ were synthesized as described previously [14]. Structural analysis was performed *via* a Panalytical Empyrean laboratory x-ray powder diffractometer. A Hitachi TM4000Plus scanning electron microscope (SEM) was used to perform energy–dispersive X–ray spectroscopy (EDS). A Quantum Design Magnetic Property Measurement System (MPMS) was used to collect magnetization data and a Quantum Design Physical Property Measurement System (PPMS) Dynacool was used for resistivity measurements. To gain insight into the electronic states of all compounds, first-principles calculations based on density functional theory (DFT) within the Vienna ab initio Simulation Package (VASP) were performed [15, 16].

RESULTS AND DISCUSSION

$AV_3Sb_{5-x}Sn_x$ all adopt the parent hexagonal $P6/mmm$ structure at room temperature, with the V atoms making up an ideal kagome network. ^{121}Sb nuclear quadrupole resonance (NQR) studies on

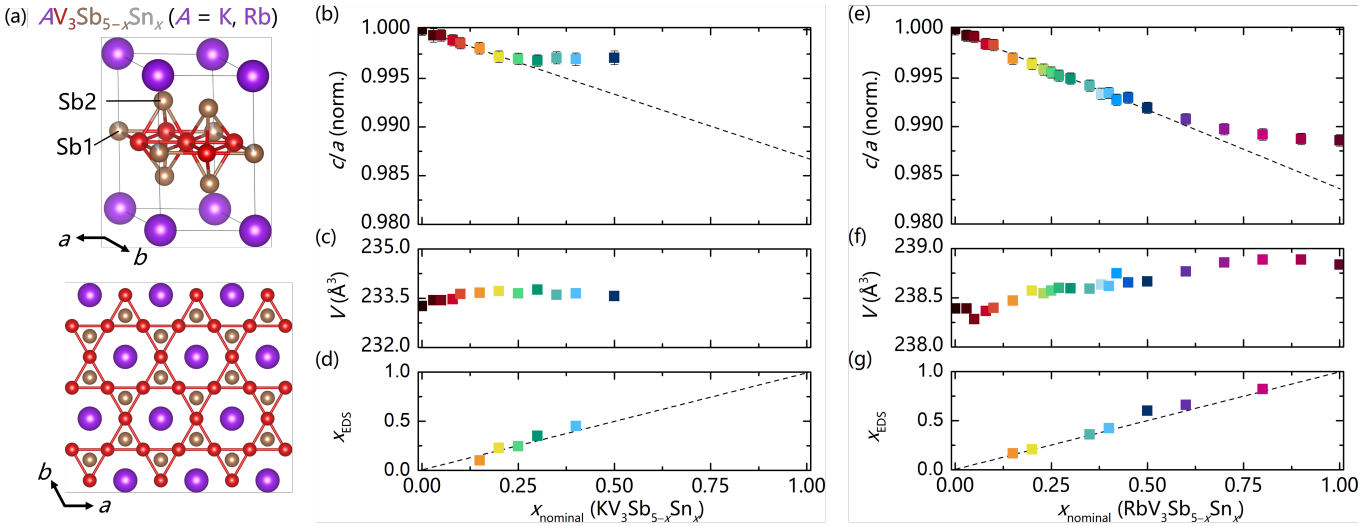

FIG. 1. (a) $AV_3Sb_{5-x}Sn_x$ crystallizes in the parent AV_3Sb_5 ($P6/mmm$) structure. Naively Sn can substitute on either the Sb1 or Sb2 sites, but from studies on $CsV_3Sb_{5-x}Sn_x$ it is clear that Sn preferentially substitutes in the in-plane kagome Sb1. (b-c) Sn integration into $KV_3Sb_{5-x}Sn_x$ causes the c/a ratio to decrease, and the solubility limit of Sn is $x \approx 0.25$, at which point the c/a ratio deviates from the linear trend. (e-f) The solubility limit of Sn in $RbV_3Sb_{5-x}Sn_x$ is a bit higher, at $x \approx 0.70$. (d, g) For samples with concentrations above the EDS sensitivity threshold, nominal Sn and measured Sn content agree. Error bars are shown unless they are smaller than associated point size.

$CsV_3Sb_{5-x}Sn_x$ have shown that the Sn atoms preferentially occupy the Sb1 sublattice site in the kagome plane [14]. Due to the similarity in structure in all of the AV_3Sb_5 structures, we assume that the Sn atoms occupy the Sb1 sublattice for A = K, Rb as well. For $KV_3Sb_{5-x}Sn_x$, polycrystalline samples were found to be single phase for $x \leq 0.25$, while for $RbV_3Sb_{5-x}Sn_x$, polycrystalline samples were single phase for $x \leq 0.7$, at which point the limit of the solid solution was reached and secondary phases were observed in both families.

The powder diffraction data was fitted using the Pawley method to study changes in unit cell as a function of Sn content. Similar to the changes observed in $CsV_3Sb_{5-x}Sn_x$, a increases as c decreases with increasing Sn content in both A = K, Rb as seen in Fig. 1(b,e), while the volume is independent of Sn content (Fig. 1(c,f)). The solubility limit of Sn is clearly reached once the c/a ratio deviates from its linear trend ($x \approx 0.30$ for $KV_3Sb_{5-x}Sn_x$ and $x \approx 0.70$ for $RbV_3Sb_{5-x}Sn_x$), and a secondary phase emerges in the powder diffraction data. EDS was performed on samples with a critical Sn content to confirm the nominal Sn content (Fig. 1(d, g)).

Single crystal KV_3Sb_5 has a superconducting T_C of 0.93 K[6]. Here, the T_C of polycrystalline KV_3Sb_5 is lower than 1.8 K, the lowest achievable temperature on the MPMS, but as Sn was incorporated, the superconducting transition temperature increases and can be detected by $x = 0.03$. Figure 2(a) shows the evolution of the superconducting transition up to $x = 0.25$, where T_C is at a maximum of 4.5 K. Beyond this Sn content, a secondary phase appears, so a suppression of superconductivity is not observed for a solid solution of $KV_3Sb_{5-x}Sn_x$. RbV_3Sb_5 shows similar behavior, with undoped crystals showing a T_C of 0.92 K[17]. Again, although the superconducting transition for RbV_3Sb_5 cannot be detected with an MPMS, by $x = 0.05$ the transition appears at 1.93 K and increases to a maximum of 4.5 K for $x = 0.40$, as seen in figure 2(c). For $x > 0.40$, T_C decreases to 3.55 K until a clear secondary phase appears. All of the superconducting volume fractions are approximately $4\pi\chi_v \approx -1$ and are normalized to -1 for ease of comparison; fractions that deviate slightly from this ideal value can be attributed to errors in packing density.

The CDW T^* was determined by looking at the inflection point of χ^{-1} *vs.* T. Polycrystalline KV_3Sb_5 as observed here has a T^* of 86 K, which is in good agreement with reported CDW transition temperatures of $\approx$ 80 K in crystals [7]. The CDW transition is quickly suppressed with increasing hole-doping, and decreases to 60 K by $x = 0.06$ and is fully suppressed by $x = 0.06$. In RbV_3Sb_5, the CDW T^* is $\approx$ 112 K, similar to the literature reported value of 110 K in single crystals [4]. The CDW is quickly suppressed to 91 K for $x = 0.10$ at which point it fully disappears (Fig. 2(d)). In both systems, the CDW transition is fully suppressed with much less Sn content than the peak of the superconductivity dome, suggesting that the interplay between superconductivity and CDW is different in A = K, Rb than in CsV_3Sb_5, where the CDW persists through the first superconducting dome. The CDW transition does not reemerge with increasing Sn content.

Electrical resistivity measurements of samples near the superconducting dome peak are shown in Figure 2(e).

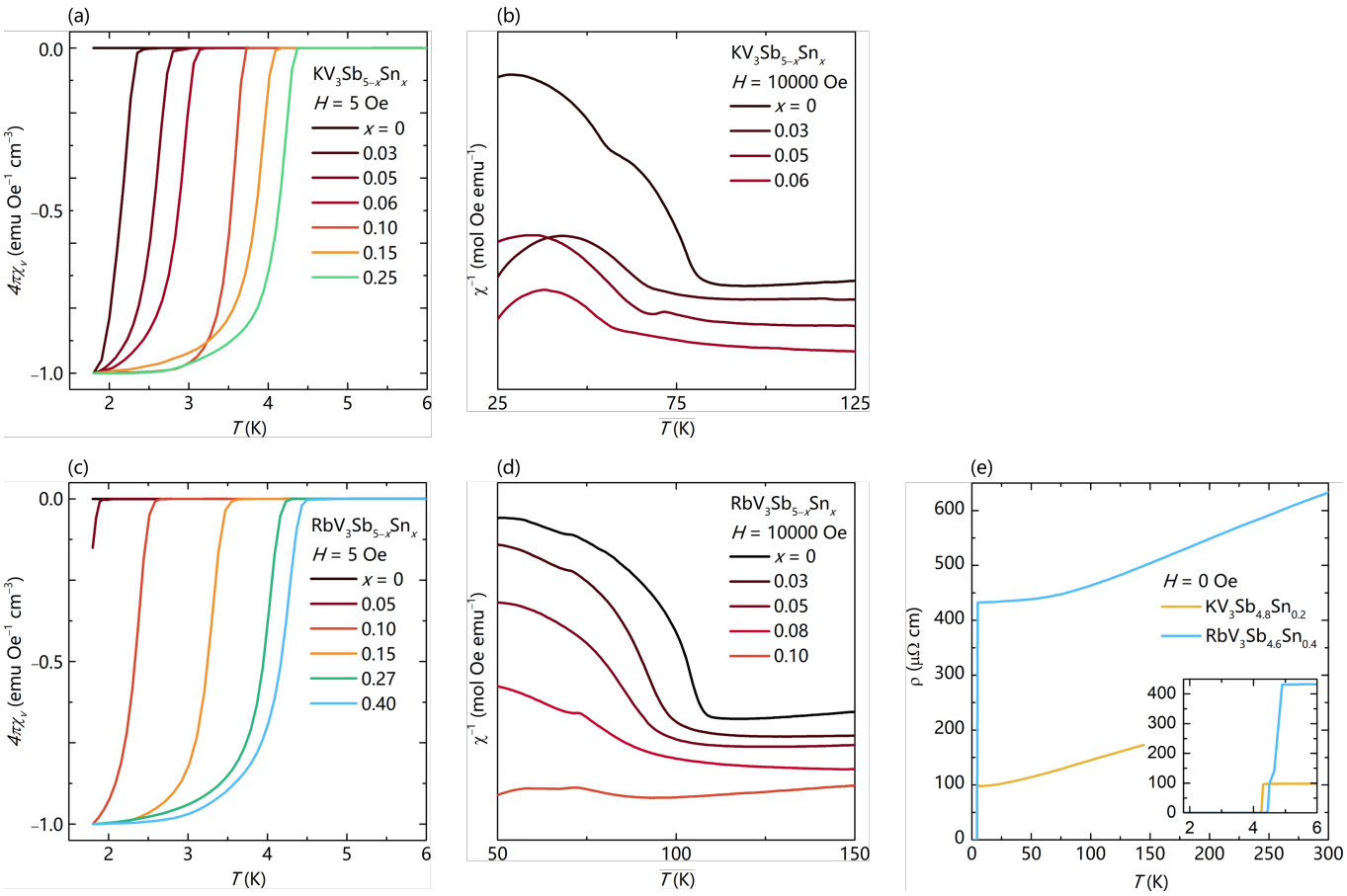

FIG. 2. (a) The superconducting T_C of $KV_3Sb_{5-x}Sn_x$ measured under a field of $H = 5$ Oe systematically shifts to higher temperature in compositions up to $x = 0.30$. The superconducting fraction is normalized to account for errors in mass and packing fraction so all data have a minimum of -1, the theoretical minimum. (b) $1/\chi$ for compositions $x \leq 0.05$ in $KV_3Sb_{5-x}Sn_x$ show the CDW T^* decreases from 86 K to 59 K and disappears for $x \geq 0.05$. (c) The superconducting T_C of $RbV_3Sb_{5-x}Sn_x$ measured under a field of $H = 5$ Oe systematically shifts to higher temperature in compositions up to $x = 0.40$. (d) $1/\chi$ for compositions $x \leq 0.10$ in $RbV_3Sb_{5-x}Sn_x$ show the CDW T^* decreases and eventually disappears for $x \geq 0.10$. (e) Resistivity data for $KV_3Sb_{4.8}Sn_{0.2}$ and $RbV_3Sb_{4.6}Sn_{0.4}$ confirm the T_C transitions and lack of CDW transitions for these higher Sn content samples.

The superconducting states are clearly observed as zero-resistivity conditions and the transitions at 4.25 K for $KV_3Sb_{4.80}Sn_{0.20}$ and 4.4 K for $RbV_3Sb_{4.60}Sn_{0.40}$ agree well with those seen in the magnetization data, while CDW transitions are not present. The residual resistance is much higher in $RbV_3Sb_{4.60}Sn_{0.40}$ and is even higher in $CsV_3Sb_{4.65}Sn_{0.35}$, suggesting an A–site dependence.

The effects of Sn-substitution on SC and CDW orders in $KV_3Sb_{5-x}Sn_x$ and $RbV_3Sb_{5-x}Sn_x$ are summarized in Figure 3. In both systems, the CDW ordering temperature is rapidly suppressed in a roughly linear fashion even with small amounts of hole doping and fully disappears before the maximum superconducting transition temperatures. The single dome nature of Sn-substituted KV_3Sb_5 and RbV_3Sb_5 is distinct from recent pressure studies that observe a double superconducting dome, with a sharp increase in T_C at very low applied pressures and a second dome emerging at much higher pressures [10, 12]. Moreover, Du *et al.* report the persistence of charge ordering at the first superconductivity peak. The differences between external pressure effects and hole-doping can be attributed to the opposite effects that these changes have to the band structures of AV_3Sb_5 compounds [8].

Due to size considerations, the solubility limits of Sn in KV_3Sb_5 and RbV_3Sb_5 are much lower than in CsV_3Sb_5. However in all of these systems, the changes in electronic structure for the compositions of interest can be extrapolated by computing band structures of substitution one Sb atom for an Sn atom within the kagome plane and out of the kagome plane. Figure 4(a) and (d) shows the band structure of undoped KV_3Sb_5 and RbV_3Sb_5, respectively, with the range of achievable Fermi levels with the loss of 1 electron per unit cell indicated in gray. Figure 4(b) and (e) show a hypothetical structure where the Sb1 lattice is fully substituted for Sn. The shifts in band structure are

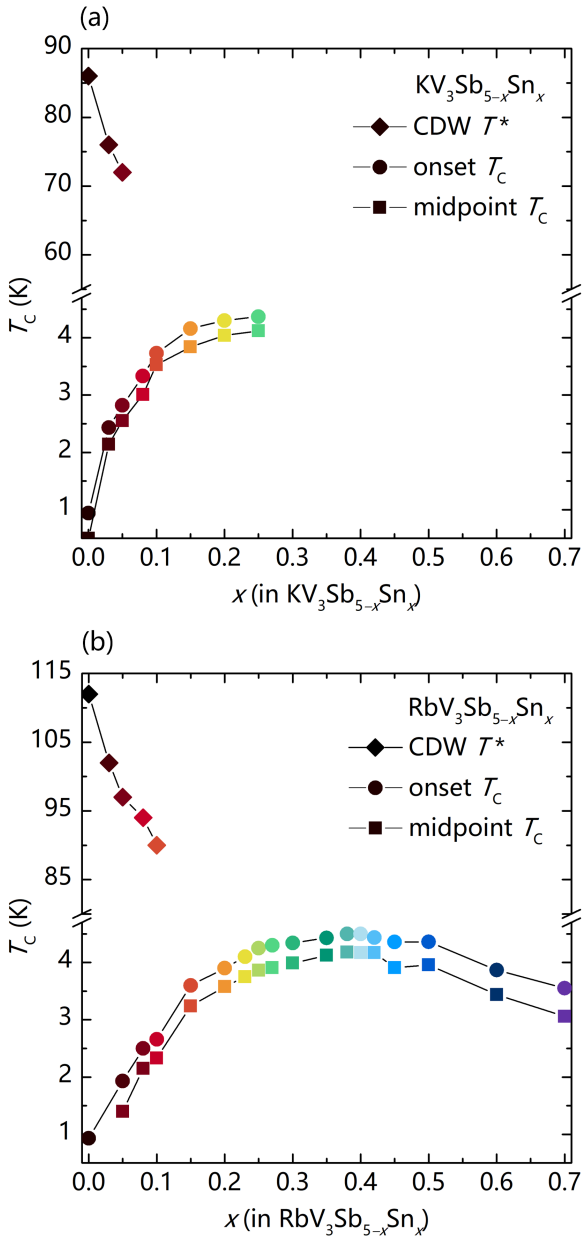

FIG. 3. The progressions of superconducting T_C and CDW temperature T^* is plotted as a function of Sn composition for $KV_3Sb_{5-x}Sn_x$ and $RbV_3Sb_{5-x}Sn_x$. In the potassium version, the solubility limit of Sn is reached before a full superconducting dome is achieved, but the suppression of CDW T^* is still fully realized. $RbV_3Sb_{5-x}Sn_x$ shows a single superconducting dome before the solubility limit is reached, with an accompanying suppressed CDW by $x = 0.1$.

similar to those seen in CsV_3Sb_4Sn, with the Γ pocket and M-point vHs lifted above the Fermi level. The calculated band structures for this structure overall suggests a rigid band shift model. Band structures for Sn substituted in the Sb2 sublattice are plotted in Figure 4(c) and (f) and show significant reconstructions at multiple points, including K, L, and H.

The changes in band structure for Sn substitution on the Sb1 sublattice in KV_3Sb_4Sn and RbV_3Sb_4Sn at first sight, appear to be very similar to those in CsV_3Sb_4Sn. However, subtle differences are evident that lead to distinct superconducting behavior. A closer examination of the saddle points around M reveals that the irreducible representations of the two points are not the same for *A* = K, Rb and Cs [8, 9]. As a consequence of the saddle point inversions, bands cross near E_F in CsV_3Sb_5 but not in KV_3Sb_5.

Hydrostatic pressure studies for AV_3Sb_5 reveal that CsV_3Sb_5 shows two superconducting T_C peaks [11] but only one peak for KV_3Sb_5 and RbV_3Sb_5 [10, 12] at low applied pressure (less than 5 GPa). Labollita *et al.* report that the vHs under hydrostatic pressure move down in energy away from E_F, and moreover the vHs points closest in energy to E_F shift uniformly (vHs1 and vHs2). Conversely, these points move up closer to E_F with hole doping, so it is interesting that similar effects are seen in the superconducting and charge density wave ordering with hydrostatic pressure and hole doping. In KV_3Sb_5, the energy of vHs2 barely changes with increased hole doping, but vHs1 increases in energy until it crosses vHs2 at a critical hole concentration. The energies of vHs2 and vHs1 have similar behavior in RbV_3Sb_5 but cross at a lower hole concentration in RbV_3Sb_5, with vHs2 starting at a slightly higher energy than vHs1 in pristine RbV_3Sb_5 and staying mostly constant with hole doping, but vHs1 increasing in energy. The energies of the two vHs points are much closer in RbV_3Sb_5 than in KV_3Sb_5. Finally, the energies of vHs1 and vHs2 are inverted in CsV_3Sb_5 (with vHs1 higher than vHs2) and both steadily increase with hole doping and never cross [8]. As holes are introduced to the system and the Γ pocket and vHs M-points are pushed up through E_F, the different band crossings for the K and Rb systems versus Cs may lead to single dome rather than double dome superconductivity behavior.

CONCLUSION

Hole-doping achieved *via* substitution of Sn on Sb sites in KV_3Sb_5 and RbV_3Sb_5 reveals similar phase diagrams consisting of a single SC dome and quickly suppressed CDW order. The V-orbital vHs are pushed up through E_F with hole-doping and likely lead to the suppression of CDW order. The Γ pocket from the Sb p_z states is quickly lifted above E_F and contributes to the enhanced superconducting T_C. In these two systems, CDW and SC order seem to be more directly in competition than in CsV_3Sb_5, although further theoretical studies are important to further clarify the differences between the three systems, especially between KV_3Sb_5 and RbV_3Sb_5. Small changes in electron count in KV_3Sb_5 and RbV_3Sb_5 achieved *via* Sn substitution dramatically affect the SC and CDW orders.

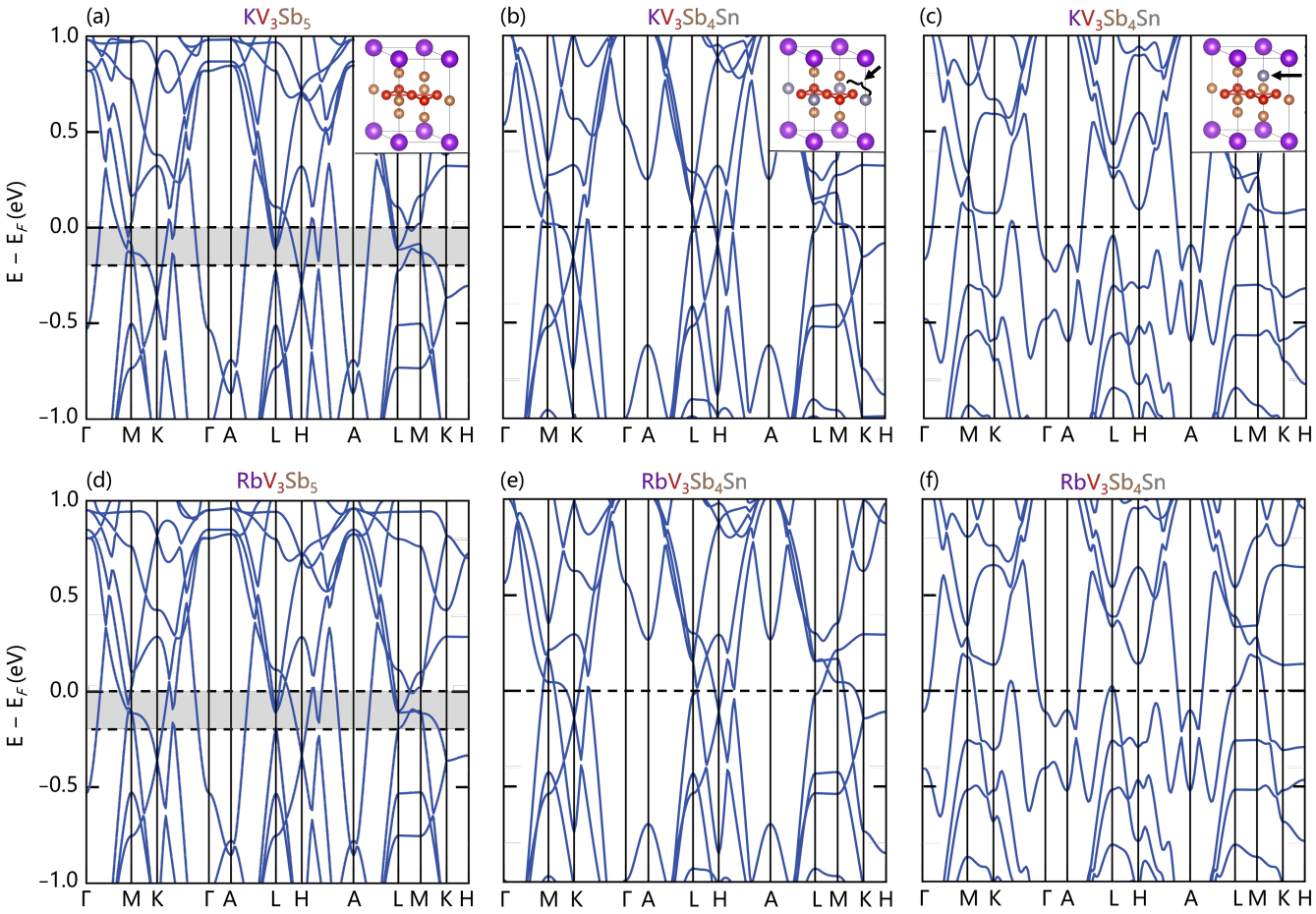

FIG. 4. (a,d) DFT calculations for KV_3Sb_5 and RbV_3Sb_5 highlighting the allowable range of Fermi levels under the rigid band approximation for substitution of one Sn atom per formula unit (one electron less Fermi energy). (b,e) Calculation for a hypothetical structure where one Sn has been substituted within the kagome plan (Sb1 sublattice). The majority of the electronic structure is preserved as KV_3Sb_5 and RbV_3Sb_5, except the Γ pocket and M point van Hove singularities which have been shifted far above and may contribute to the changing observable properties. (c,f) Calculation for a hypothetical structure where one Sn has been substituted out of the kagome plane (Sb2 sublattice). Here a strong reconstruction of many bands can be observed, in particular near K, H, and K-Γ.

ACKNOWLEDGMENTS

This work was supported by the National Science Foundation (NSF) through Enabling Quantum Leap: Convergent Accelerated Discovery Foundries for Quantum Materials Science, Engineering and Information (Q-AMASE-i): Quantum Foundry at UC Santa Barbara (DMR-1906325). The research reported here made use of shared facilities of the NSF Materials Research Science and Engineering Center at UC Santa Barbara DMR-1720256, a member of the Materials Research Facilities Network (www.mrfn.org). Use of the Advanced Photon Source at Argonne National Laboratory was supported by the U.S. Department of Energy, Office of Science, Office of Basic Energy Sciences, under Contract No. DE-AC02-06CH11357. YMO is supported by the National Science Foundation Graduate Research Fellowship Program under Grant No. DGE-1650114. BRO is supported by the California NanoSystems Institute through the Elings Fellowship program. FK acknowledges the Roy T. Eddleman Center for Quantum Innovation (ECQI) for their support.

REFERENCES

* yoey@ucsb.edu

[1] H.-M. Guo and M. Franz, Topological insulator on the kagome lattice, Phys. Rev. B **80**, 113102 (2009).
[2] W.-H. Ko, P. A. Lee, and X.-G. Wen, Doped kagome system as exotic superconductor, Phys. Rev. B **79**, 214502 (2009).

[3] E. Liu, Y. Sun, N. Kumar, L. Muechler, A. Sun, L. Jiao, S.-Y. Yang, D. Liu, A. Liang, Q. Xu, *et al.*, Giant anomalous Hall effect in a ferromagnetic kagome-lattice semimetal, Nat. Phys. **14**, 1125 (2018).

[4] B. R. Ortiz, L. C. Gomes, J. R. Morey, M. Winiarski, M. Bordelon, J. S. Mangum, I. W. Oswald, J. A. Rodriguez-Rivera, J. R. Neilson, S. D. Wilson, *et al.*, New kagome prototype materials: discovery of KV_3Sb_5, RbV_3Sb_5, and CsV_3Sb_5, Phys. Rev. Mater. **3**, 094407 (2019).

[5] B. R. Ortiz, S. M. Teicher, Y. Hu, J. L. Zuo, P. M. Sarte, E. C. Schueller, A. M. Abeykoon, M. J. Krogstad, S. Rosenkranz, R. Osborn, R. Seshadri, L. Balents, J. He, and S. D. Wilson, CsV_3Sb_5: A $\mathbb{Z}_2$ topological kagome metal with a superconducting ground state, Phys. Rev, Lett. **125**, 247002 (2020).

[6] B. R. Ortiz, P. M. Sarte, E. M. Kenney, M. J. Graf, S. M. Teicher, R. Seshadri, and S. D. Wilson, Superconductivity in the $\mathbb{Z}_2$ kagome metal KV_3Sb_5, Phys. Rev. Mater. **5**, 034801 (2021).

[7] Y.-X. Jiang, J.-X. Yin, M. M. Denner, N. Shumiya, B. R. Ortiz, G. Xu, Z. Guguchia, J. He, M. S. Hossain, X. Liu, *et al.*, Unconventional chiral charge order in kagome superconductor KV_3Sb_5, Nat. Mater. , 1 (2021).

[8] H. LaBollita and A. S. Botana, Tuning the Van Hove singularities in AV_3Sb_5 (A= K, Rb, Cs) via pressure and doping, Physical Review B **104**, 205129 (2021).

[9] E. Uykur, B. Ortiz, O. Iakutkina, M. Wenzel, S. Wilson, M. Dressel, and A. Tsirlin, Low-energy optical properties of the nonmagnetic kagome metal CsV_3Sb_5, Physical Review B **104**, 045130 (2021).

[10] F. Du, S. Luo, B. R. Ortiz, Y. Chen, W. Duan, D. Zhang, X. Lu, S. D. Wilson, Y. Song, and H. Yuan, Pressure-induced double superconducting domes and charge instability in the kagome metal KV_3Sb_5, Phys. Rev. B **103**, L220504 (2021).

[11] K. Chen, N. Wang, Q. Yin, Y. Gu, K. Jiang, Z. Tu, C. Gong, Y. Uwatoko, J. Sun, H. Lei, *et al.*, Double superconducting dome and triple enhancement of T_C in the kagome superconductor CsV_3Sb_5 under high pressure, Phys. Rev. Lett. **126**, 247001 (2021).

[12] C. Zhu, X. Yang, W. Xia, Q. Yin, L. Wang, C. Zhao, D. Dai, C. Tu, B. Song, Z. Tao, *et al.*, Double-dome superconductivity under pressure in the V-based kagome metals AV_3Sb_5 (A = Rb and K), Physical Review B **105**, 094507 (2022).

[13] F. Yu, D. Ma, W. Zhuo, S. Liu, X. Wen, B. Lei, J. Ying, and X. Chen, Unusual competition of superconductivity and charge-density-wave state in a compressed topological kagome metal, Nature communications **12**, 1 (2021).

[14] Y. M. Oey, B. R. Ortiz, F. Kaboudvand, J. Frassineti, E. Garcia, S. Sanna, V. Mitrović, R. Seshadri, and S. D. Wilson, Fermi level tuning and double-dome superconductivity in the kagome metals $CsV_3Sb_{5-x}Sn_x$, Phys. Rev. Mater. **6** (2022).

[15] G. Kresse and J. Furthmüller, Efficient iterative schemes for ab initio total-energy calculations using a plane-wave basis set, Phys. Rev. B **54**, 11169 (1996).

[16] G. Kresse and J. Furthmüller, Efficiency of ab-initio total energy calculations for metals and semiconductors using a plane-wave basis set, Comput. Mater. Sci. **6**, 15 (1996).

[17] Q. Yin, Z. Tu, C. Gong, Y. Fu, S. Yan, and H. Lei, Superconductivity and normal-state properties of kagome metal RbV_3Sb_5 single crystals, Chinese Phys. Lett. **38**, 037403 (2021).